

SUPPLEMENTARY MATERIAL

On the behaviour of structure-sensitive reactions on single atom and highly dilute alloy surfaces

Konstantinos G. Papanikolaou and Michail Stamatakis*

Thomas Young Centre and Department of Chemical Engineering, University College London,

Roberts Building, Torrington Place, London WC1E 7JE, UK

***Corresponding Author:** m.stamatakis@ucl.ac.uk

I. K-point convergence testing

The Monkhorst-Pack k-mesh for our DFT calculations was chosen after performing preliminary k-point convergence testing. The parameter that was converged with respect to the k-mesh was the adsorption energy of atomic hydrogen (i.e. $E_{\text{ads}}(\text{H})$) on Cu(100) and Pt/Cu(100). To this end, we computed $E_{\text{ads}}(\text{H})$ on a 4-fold site of a Cu(100) surface, on the dopant top site of a Pt/Cu(100) surface and on a mixed bridge site of the same surface for a number of k-point meshes. Moreover, we compare the computed adsorption energies of CO with $9 \times 9 \times 1$ and $13 \times 13 \times 1$ k-meshes on the top site of four random (111) – (Figure S2). The results are shown in Figure S1 and Figure S2 indicating that a $9 \times 9 \times 1$ k-mesh affords enough accuracy, which is identical to the accuracy provided by a $13 \times 13 \times 1$ k-mesh.

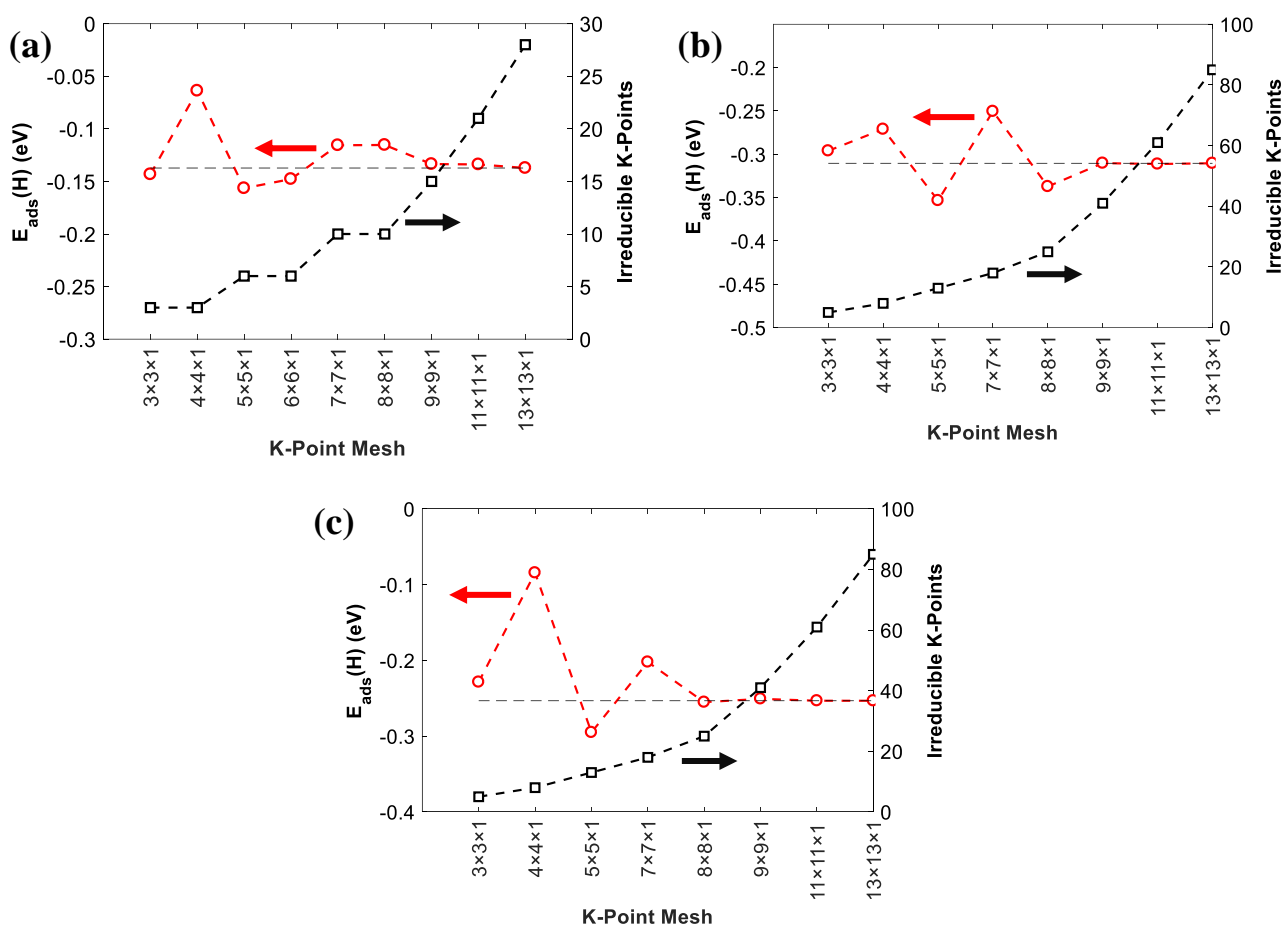


Figure S1. K-point convergence test for a H adatom on (a) a 4-fold site on Cu(100); (b) a mixed bridge site on a Pt/Cu(100) SAA surface, and (c) a dopant top site of the latter surface.

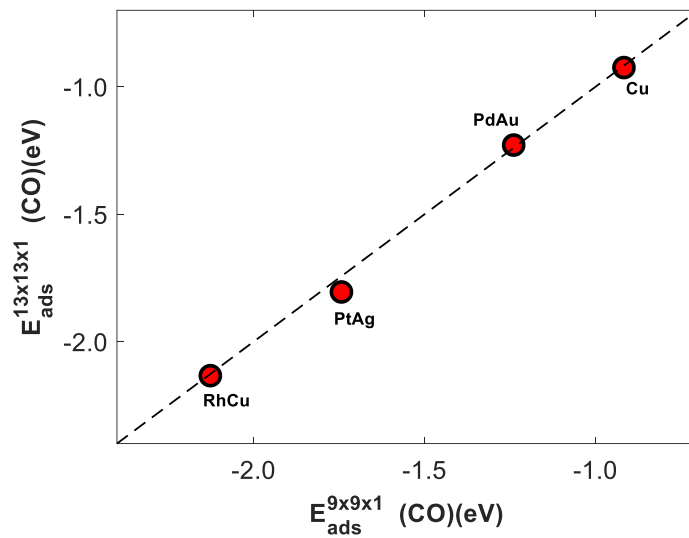


Figure S2. Parity between the adsorption energies of CO computed with $9 \times 9 \times 1$ and $13 \times 13 \times 1$ k-meshes. CO is chemisorbed on the top dopant sites of the single atom alloy surfaces and on a top site on the Cu(111) surface.

II. Correlation plots between adsorption energy and d band centre

By plotting the adsorption energy of different species (E_{ads}) versus the d band centre (ϵ_d) of the d states of the single dopant atoms, we realise that the reactivity of SAA surfaces does not follow the conventional d band model.¹ We have computed the adsorption energy of O, N₂ and NO species adsorbed on the dopant top site of a number of SAA surfaces, which have Pt, Pd, Rh or Ni as dopant and Cu, Au or Ag as host (Figure S3). In general, we determine that there is a poor correlation between E_{ads} and ϵ_d for both SAA (100) and (111) surfaces. This observation furnishes evidence that the behaviour of SAAs deviates from the d band model and is in agreement with previous computational works.¹

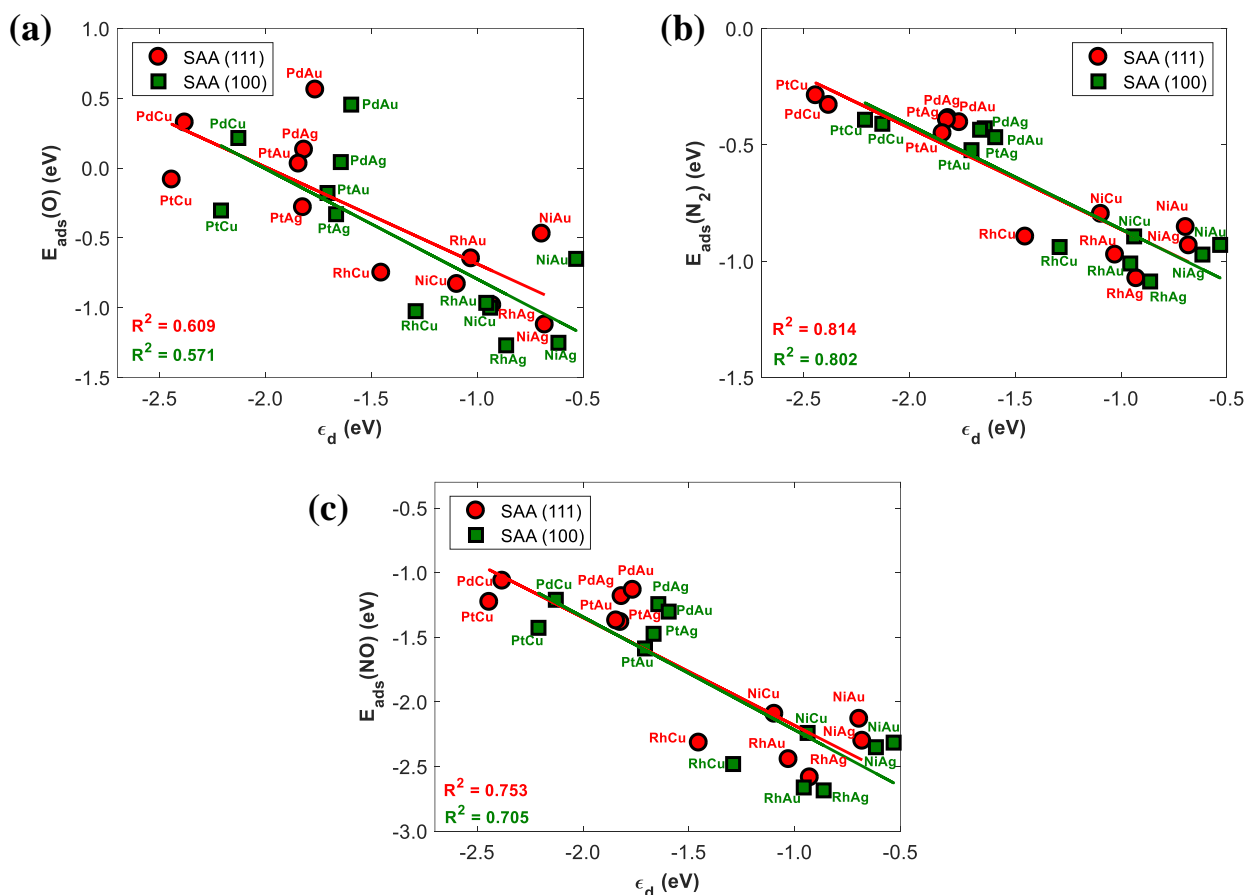


Figure S3. Linear correlation between the adsorption energy of (a) O; (b) N₂ and (c) NO on the dopant top site of several SAA surfaces and ϵ_d . Regression lines are shown with the corresponding coefficients of determination (R^2).

III. Brønsted–Evans–Polanyi relationships

The Brønsted-Evans-Polanyi (BEP) relationships for each studied reaction on single atom alloy (SAA) and pure metal surfaces are displayed in Figure S4. We note the BEP relation for the dissociation of CO₂ on SAA (111) surfaces is presented elsewhere.²

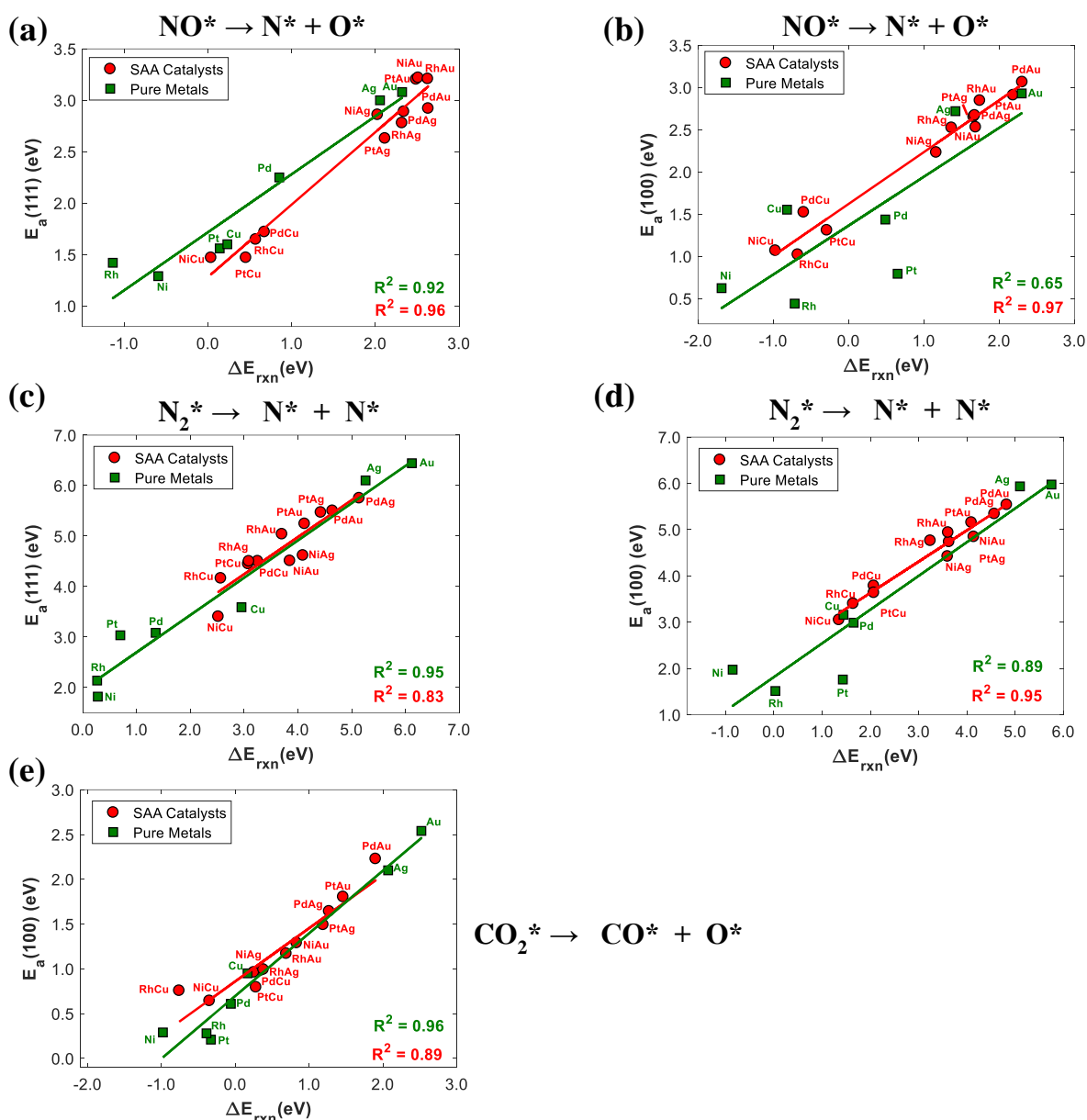


Figure S4. BEP relations for (a) the dissociation of NO on (111) surfaces; (b) the dissociation of NO on (100) surfaces; (c) the dissociation of N₂ on (111) surfaces; (d) the dissociation of N₂ on (100) surfaces and (e) the CO₂ dissociation reaction on (100) surfaces. The surfaces include SAAs (red circles) and pure metals (green squares). Regression lines and the corresponding coefficients of determination (R^2) are shown in each plot.

IV. Activation barriers for the CO oxidation reaction

The kinetic barriers for the catalytic CO oxidation on SAA, pure metal, and Ni ensemble (i.e. Ni₂Cu and Ni₃Cu) surfaces are shown in the parity plot of Figure S5. We note that the oxidation of CO is an important step for the NO + CO reaction, and therefore a successful NO reduction catalyst should exhibit low kinetic barriers for this reaction step.

We find that the CO oxidation reaction is relatively facile on Cu(111) and Cu(100) surfaces, which exhibit kinetic barriers of 0.48 eV and 0.73 eV, respectively (Figure S5). This observation, in combination with the relatively low barriers for the activation of N=O chemical bonds by Ni₃Cu and Ni₂Cu, makes us envision a bifunctional dilute Ni/Cu alloy for the NO + CO chemistry. On this alloy surface, the oxidation of CO may be happening on Cu sites, whereas Ni ensembles will serve as the active sites for the activation of chemical bonds as well as for the efficient formation and removal of N₂ (see the main text).

We also note that the CO oxidation reaction is extremely facile on Ag and Au surfaces (Figure S5). Similarly, Ag- and Au-based SAA surfaces exhibit low kinetic barriers toward the same reaction (Figure S5). Yet, all these surfaces have shown very poor performance in cleaving chemical bonds (see the main text).

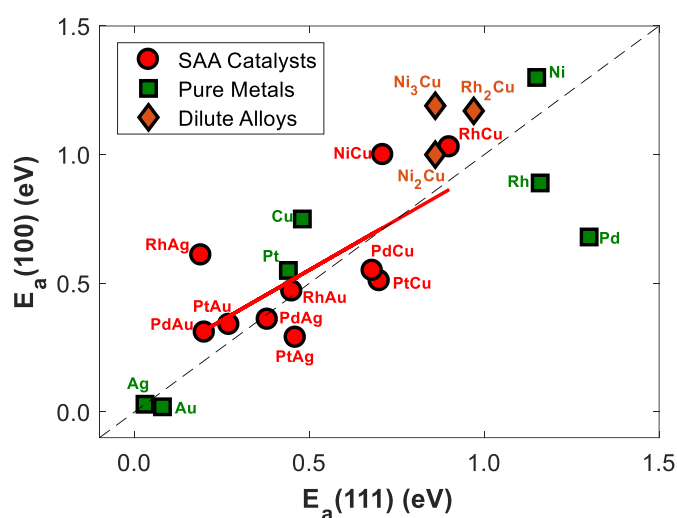


Figure S5. $E_a(100)$ and $E_a(111)$ parity for SAA surfaces (red circles), pure metal surfaces (green squares) and Ni ensembles on Cu (orange diamonds) for the catalytic CO oxidation. The black dashed line represents the parity line.

V. Initial final and transition state structures on SAA and dilute alloy surfaces

In this section we provide images of the initial state (IS), final state (FS) and transition state (TS) structures for the examined dissociation reactions in the main text.

- **NO dissociation- SAA surfaces**

On Au-based (100) SAA surfaces, the IS of the dissociation of NO reaction involves a nitric oxide molecule adsorbed in an upright structure on the top dopant site (Figure S6 (a)). In the TS, NO is tilted parallel to the surface with N adsorbed on a mixed bridge site and O close to mixed 4-fold site (Figure S6 (a)). In the FS, N is moved near to a mixed 4-fold site, while O remains in the same position as in the TS structure (Figure S6 (a)). The only exception to this is the Ni/Au(100) surface (Figure S6 (b)). For all Ag-based surfaces we note that the IS, TS and FS are similar to those of Au-based (100) surfaces (Figure S6 (c)). In contrast, on Cu-based (100) surfaces the IS includes an NO molecule adsorbed on a mixed 4-fold site, while the TS and FS resemble, to some extent, to those of Au- and Ag-based surfaces (Figure S6 (d)).

Figure S7 shows the top view of the corresponding IS, TS and FS structures on SAA (111) surfaces. We point out that in the TS and FS structures N and O adatoms generally prefer hollow sites (i.e. 2-fold and 3-fold). Our results for Cu-based (111) surfaces are in line with previously reported findings.¹ Finally, Figure S8 displays the same structures as in Figure S6 and Figure S7, but for the Ni ensemble (100) and (111) surfaces (i.e. Ni₂Cu and Ni₃Cu). On the latter surfaces, the N=O bond is cleaved above a hollow site surrounded by Ni atoms, thereby resulting in N and O adatoms on mixed 3-fold sites for (111) surfaces or mixed 4-fold sites for (100) sites.

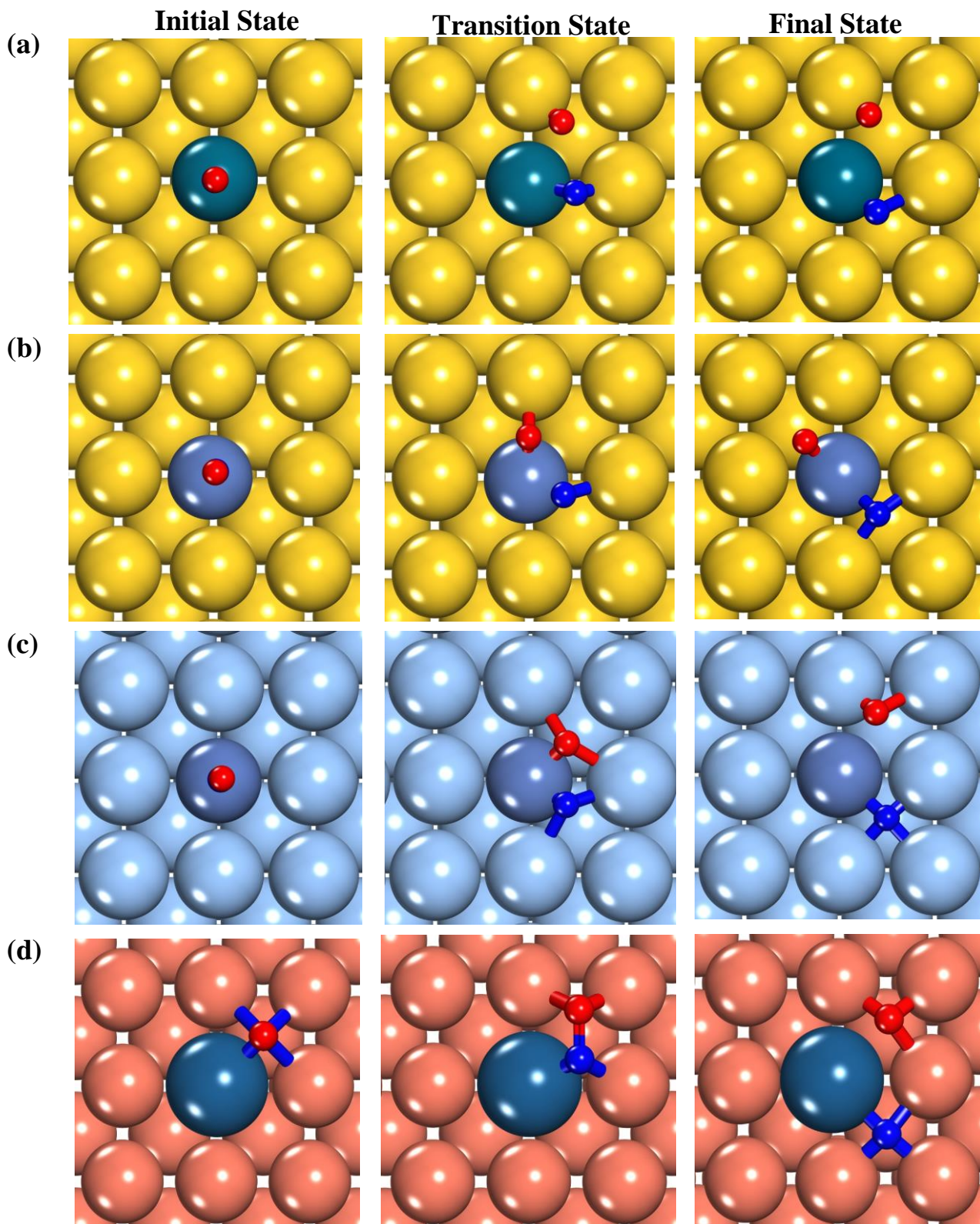


Figure S6. IS, TS and FS structures for the NO dissociation reaction on (a) Pd/Ah SAA (100) surface, which is representative for Au-based surfaces except for Ni/Au(100); (b) the Ni/Au(100) surface; (c) Ni/Ag SAA (100), and (d) Ni/Cu SAA (100), which are representative of Ag- and Cu-based SAA surfaces, respectively. O and N atoms are shown in red and blue, while Cu, Ag and Au atoms are shown in orange, light blue and yellow, respectively. The dopant atoms are shown in dark colours (dark blue or green and purple).

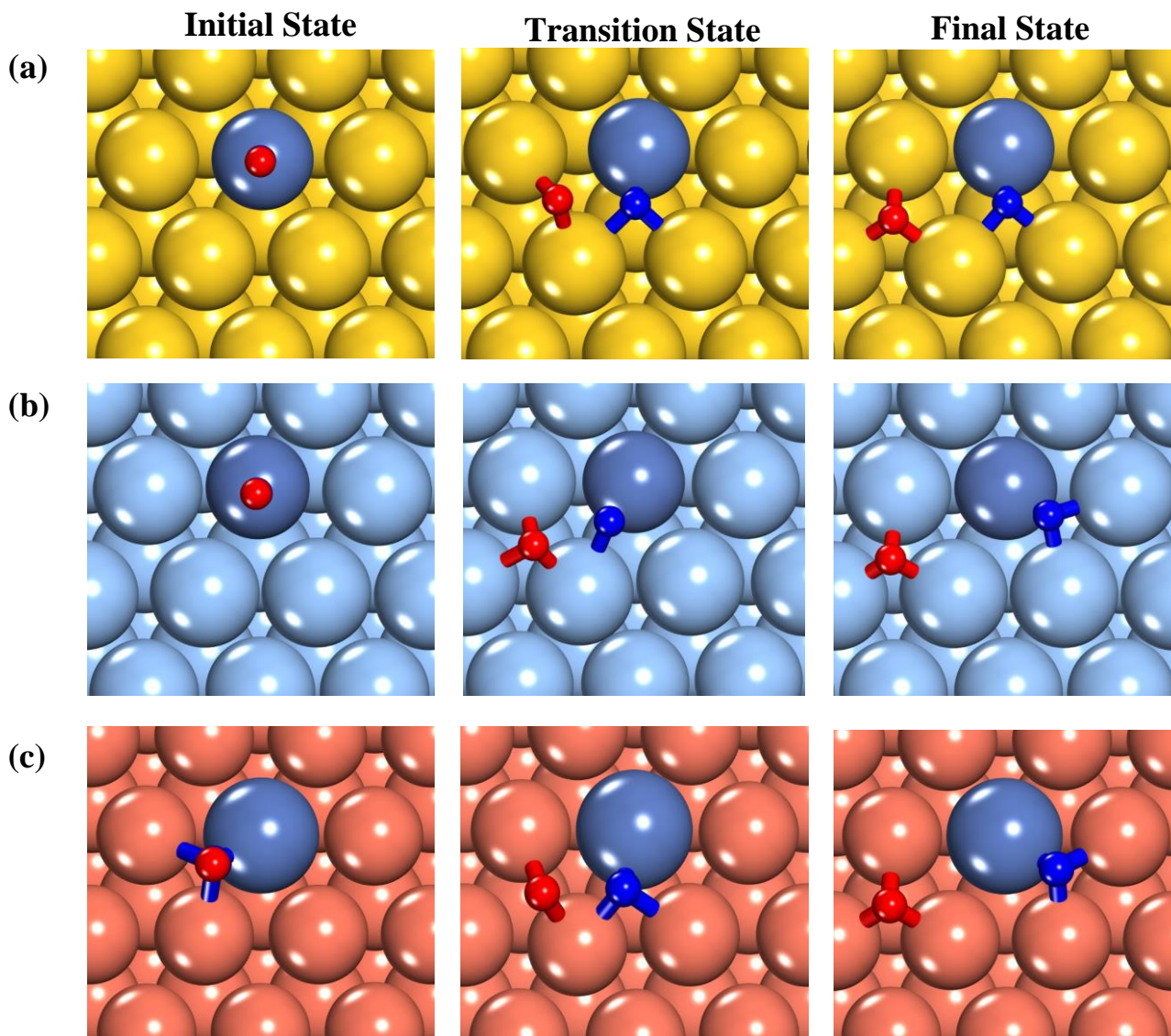


Figure S7. Representative IS, TS and FS structures for the NO dissociation reaction on (a) Au-based SAA (111) surfaces; (b) Ag-based SAA (111) surfaces, and (c) Cu-based SAA (111) surfaces. O and N atoms are shown in red and blue, respectively. Cu, Ag and Au atoms are shown in orange, light blue and yellow, respectively. Ni atoms are shown in purple; however, the displayed structures are indicative of the IS, FS and TS structures for other SAA(111) surfaces.

- NO dissociation- Ni ensemble surfaces

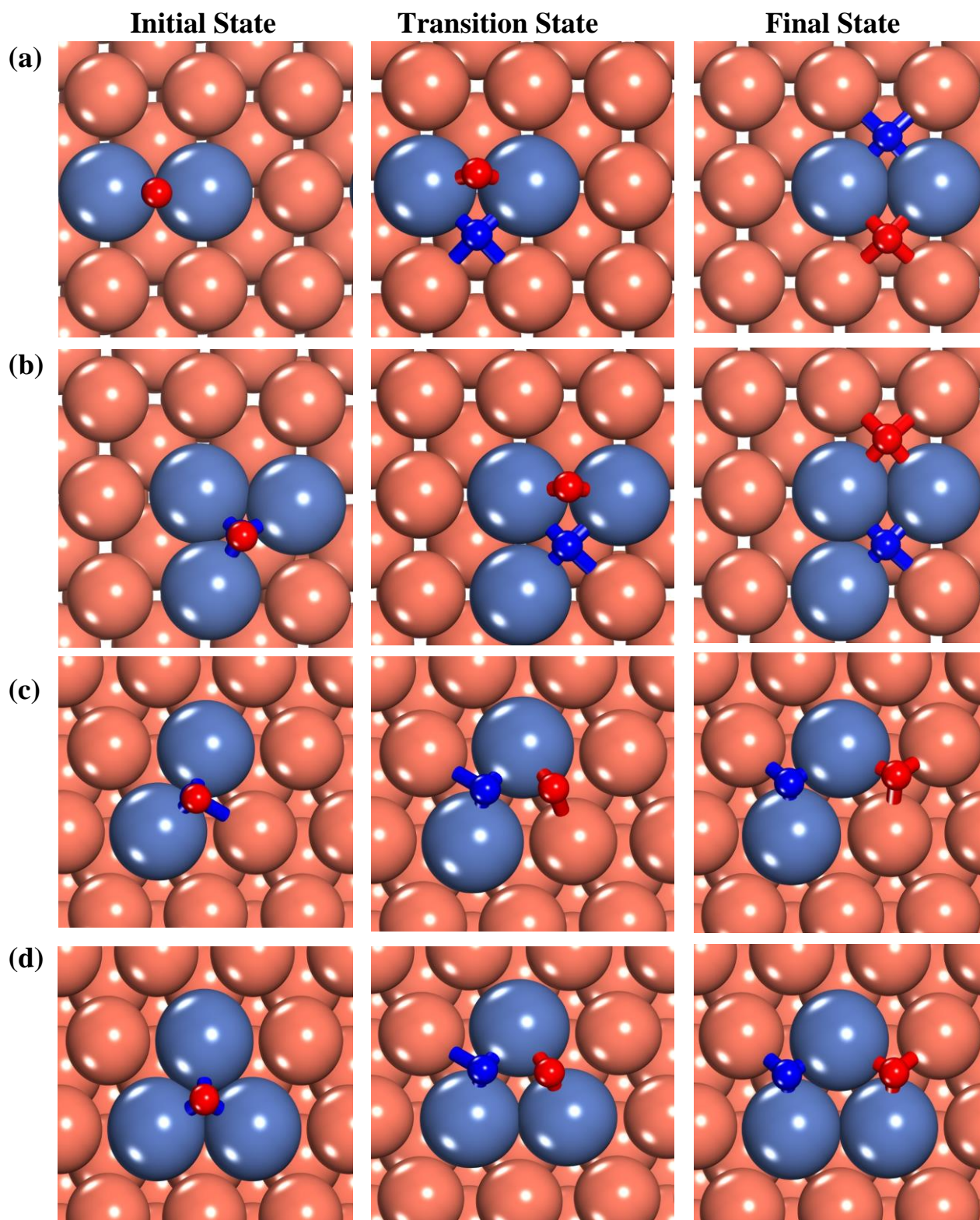


Figure S8. IS, TS and FS structures for the NO dissociation reaction on the (a) $\text{Ni}_2\text{Cu}(100)$ surface; (b) the $\text{Ni}_3\text{Cu}(100)$ surface; (c) the $\text{Ni}_2\text{Cu}(111)$ surface and (d) the $\text{Ni}_3\text{Cu}(111)$ surface. O and N atoms are shown in red and blue, respectively. Cu, Ag and Au atoms are shown in orange, light blue and yellow, respectively. The dopant atoms are shown in purple.

Table S1. Summary of adsorption energies of NO on the most stable adsorption site of Ni dimers and trimers embedded on Cu surfaces. The most stable adsorption sites are hollow bridge and threefold sites for Ni dimers and trimers, respectively, and NO is perpendicular to the surface as shown in Figure S8.

Alloy Surface	$E_{\text{ads}}(\text{NO})$ (111) (eV)	$E_{\text{ads}}(\text{NO})$ (100) (eV)
Ni₂Cu	-2.65	-2.86
Ni₃Cu	-3.07	-3.09
Cu	-1.55	-1.61
Ni	-2.84	-2.99

- **CO₂ dissociation- SAA surfaces**

The IS, TS and FS structures for the dissociation of CO₂ on SAA(100) and Ni ensemble surfaces (including (100) and (111) surfaces) are shown in Figure S9 and Figure S10, respectively. Herein, we do not show images of the IS, FS and TS structures for SAA(111) surfaces as such images are provided elsewhere.² The IS state can be either a physisorbed CO₂ molecule, which is parallel to the surface (Figure S11 (a)) or a chemisorbed “bent” CO₂ molecule in a η^2 -(atop, atop) adsorption mode (Figure S11 (a)). We determine that the latter “bent structure” is thermodynamically more stable than the physisorbed structure for a number of (100) surfaces (Table S2) and for all Ni₂Cu and Ni₃Cu surfaces (Table S4). The high stability of the η^2 -(atop, atop) adsorption mode on Ni ensembles is a testament to the significant interaction between Ni₂Cu and Ni₃Cu surfaces, thereby leading to low CO₂ dissociation kinetic barriers (see the main text). Conversely, the physisorbed structure is preferred on all (111) surfaces with the only exceptions being the Rh(111) and Rh/Ag(111) surfaces (Table S3).

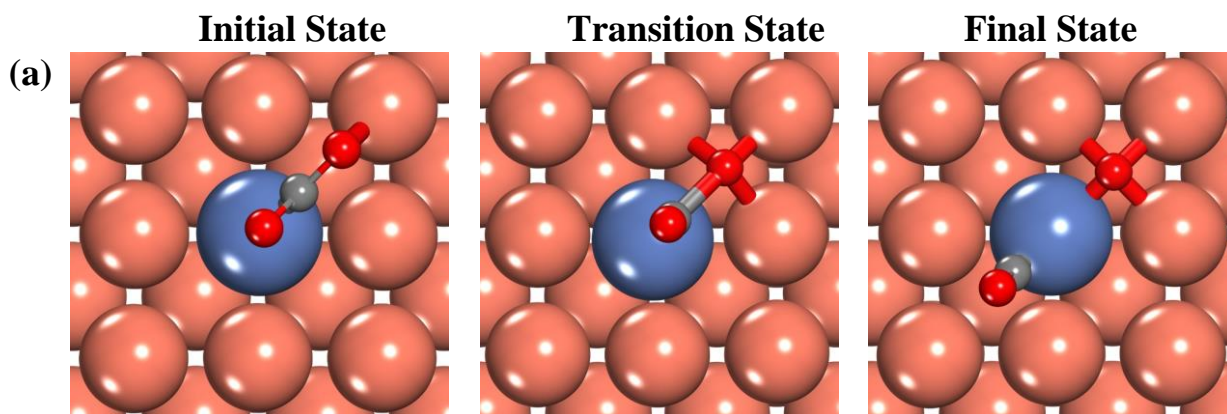


Figure S9. IS, TS and FS structures for the CO₂ dissociation reaction on SAA (100) surfaces. The IS, FS and TS structures are similar for Cu-, Ag- and Au-based SAA surfaces. O and C atoms are shown in red and grey, respectively. The dopant and host metal atoms are shown in orange and purple, respectively.

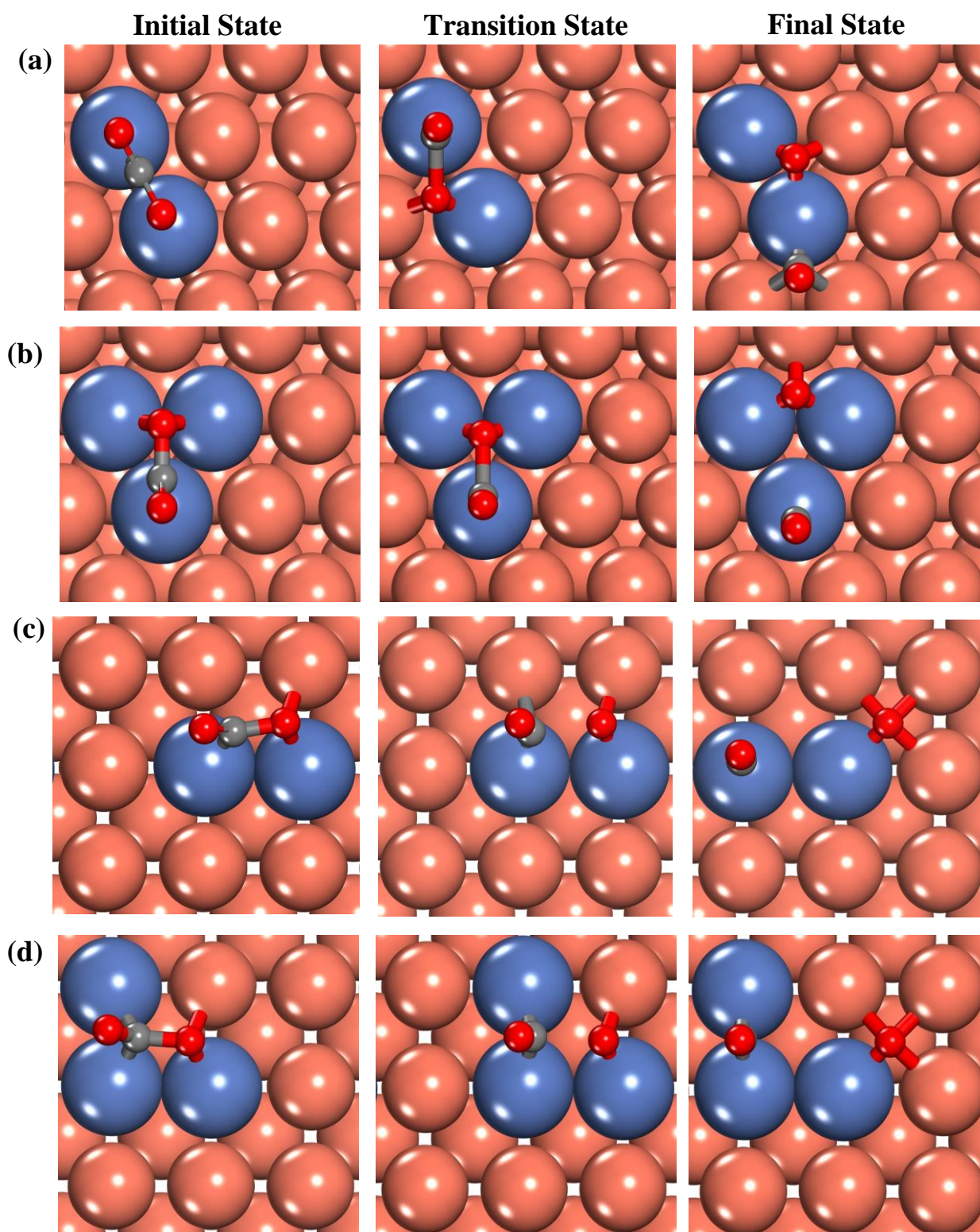


Figure S10. IS, TS and FS structures for the CO₂ dissociation reaction on (a) Ni₂Cu(111); (b) Ni₃Cu(111); (c) Ni₂Cu(100) and (d) Ni₃Cu(100). O and C atoms are shown in red and grey, respectively. The dopant and Cu atoms are shown in orange and purple, respectively.

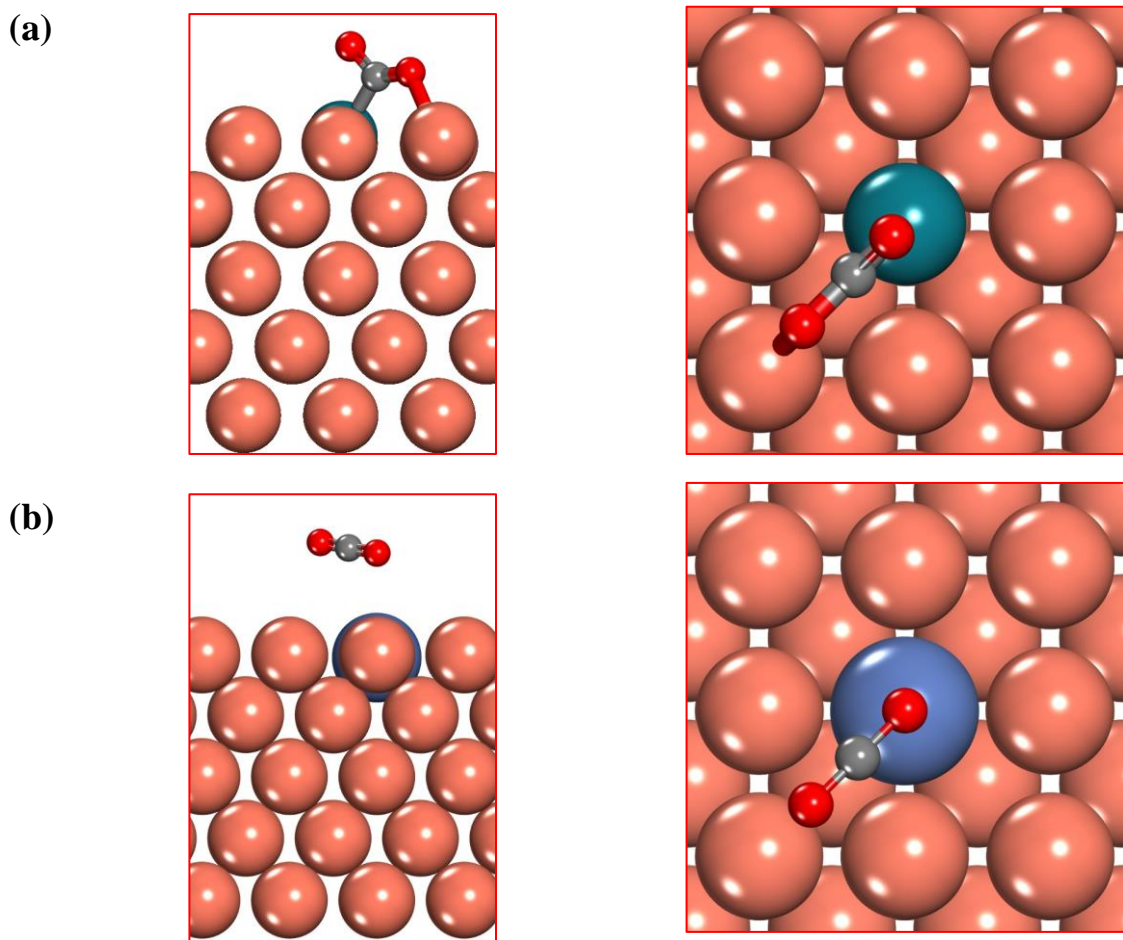


Figure S11. (a) The side and top views of the η^2 -(atop, atop) CO₂ adsorption structure on a Rh/Cu(100) SAA surface. (b) The side and top views of the CO₂ physisorbed structure on a Ni/Cu(100) SAA surface. O and C atoms are shown in red and grey, respectively. Ni, Rh and Cu atoms are shown in purple, green and orange, respectively.

Table S2. Summary of CO₂ adsorption energies for the physisorbed and η^2 -(atop, atop) structures on the investigated (100) surfaces. A dash implies that the specific adsorption structure is not a minimum in the potential energy surface.

Catalyst Surface	E _{ads} (CO ₂) (eV)	
	Physisorbed Structure	“Bent” Structure (η^2 -(atop, atop))
NiAg(100)	-0.26	-0.42
NiAu(100)	-0.31	-0.20
NiCu(100)	-0.26	-0.42
PdAg(100)	-0.26	-0.23
PdAu(100)	-0.30	—
PdCu(100)	-0.26	-0.11
PtAg(100)	-0.28	-0.37
PtAu(100)	-0.27	—
PtCu(100)	-0.26	-0.27
RhAg(100)	-0.27	-0.60
RhAu(100)	-0.33	-0.27
RhCu(100)	-0.29	-0.57
Pt(100)	-0.27	-0.20
Ni(100)	-0.26	-0.77
Rh(100)	-0.29	-0.66
Au(100)	-0.26	—
Ag(100)	-0.25	—
Cu(100)	-0.24	0.01
Pd(100)	-0.29	-0.30

Table S3. Summary of CO₂ adsorption energies for the physisorbed and η^2 -(atop, atop) structures on the investigated (111) surfaces. Dashes imply that the specific adsorption structure is not a minimum in the potential energy surface.

Catalyst Surface	E _{ads} (CO ₂) (eV)	
	Physisorbed Structure	“Bent” Structure (η^2 -(atop, atop))
NiAg(111)	-0.20	-0.16
NiAu(111)	-0.27	—
NiCu(111)	-0.28	-0.12
PdAg(111)	-0.22	-0.004
PdAu(111)	-0.26	—
PdCu(111)	-0.28	0.12
PtAg(111)	-0.22	-0.08
PtAu(111)	-0.25	—
PtCu(111)	-0.28	0.003
RhAg(111)	-0.19	-0.38
RhAu(111)	-0.15	-0.05
RhCu(111)	-0.28	-0.22
Pt(111)	-0.36	0.15
Ni(111)	-0.16	0.20
Rh(111)	-0.25	-0.27
Au(111)	-0.22	—
Ag(111)	-0.26	—
Cu(111)	-0.30	0.34
Pd(111)	-0.17	-0.04

Table S4. Summary of CO₂ adsorption energies for the physisorbed and η^2 -(atop, atop) structures on the Ni ensemble (111) surfaces.

Catalyst Surface	E _{ads} (CO ₂) (eV)	E _{ads} (CO ₂) (eV)
	Physisorbed Structure	“Bent” Structure (η^2 -(atop, atop))
Ni₂Cu(111)	-0.26	-0.37
Ni₃Cu(111)	-0.27	-0.43
Ni₂Cu(100)	-0.26	-0.65
Ni₃Cu(100)	-0.27	-0.87

- **N₂ dissociation- SAA surfaces**

Figure S12 shows the top view of the IS, TS and FS structures for the dissociation of N₂ reaction on SAA (100) and (111). Herein, we present these structures for Cu-based surfaces only, but we find that the corresponding structures on Au- and Ag-based alloys are almost identical to those for Cu-based alloys. In general, N₂ is adsorbed on the dopant top site in an upright adsorption mode and after the dissociation N adatoms are located in hollow sites. In addition, we present the same structures for Ni ensemble surfaces in Figure S13.

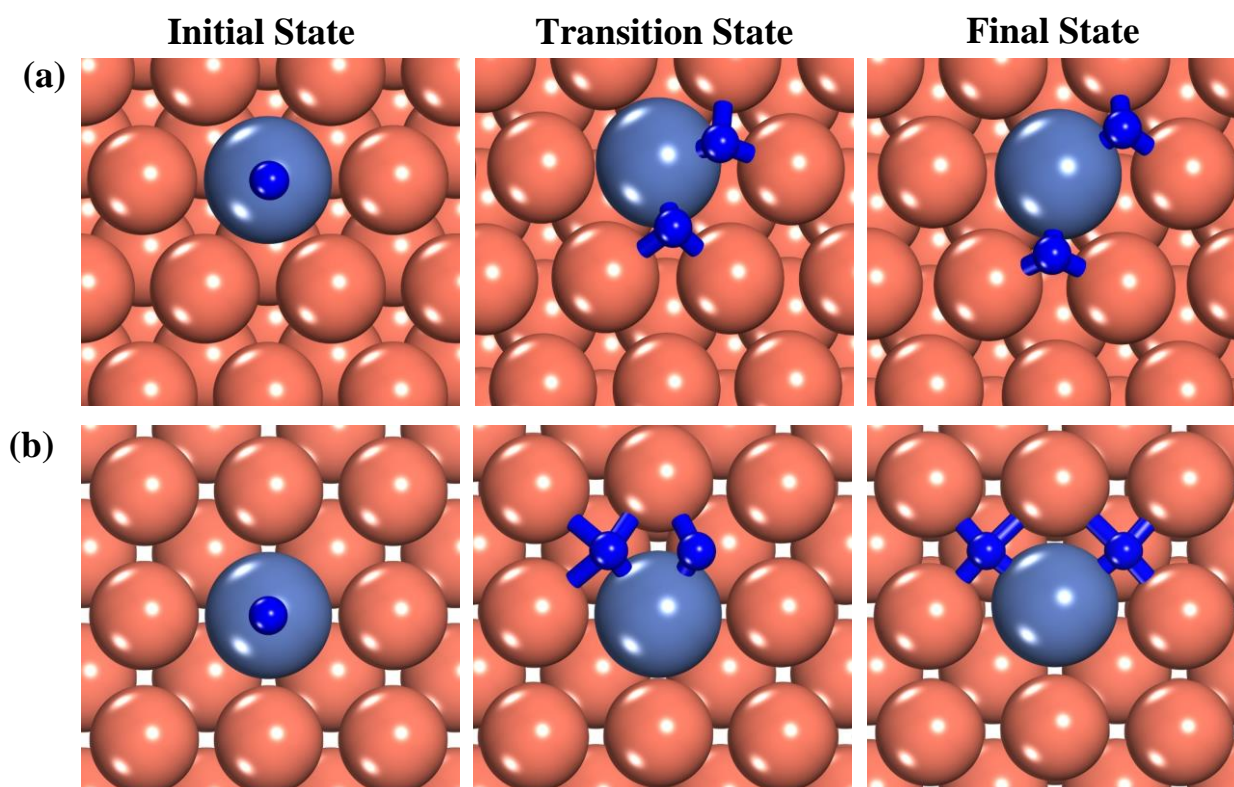


Figure S12. IS, TS and FS structures for the N_2 dissociation reaction on (a) SAA(111) surfaces, and (b) SAA(100) surfaces. N atoms are shown in blue. The dopant and host metal atoms are shown in purple and orange, respectively.

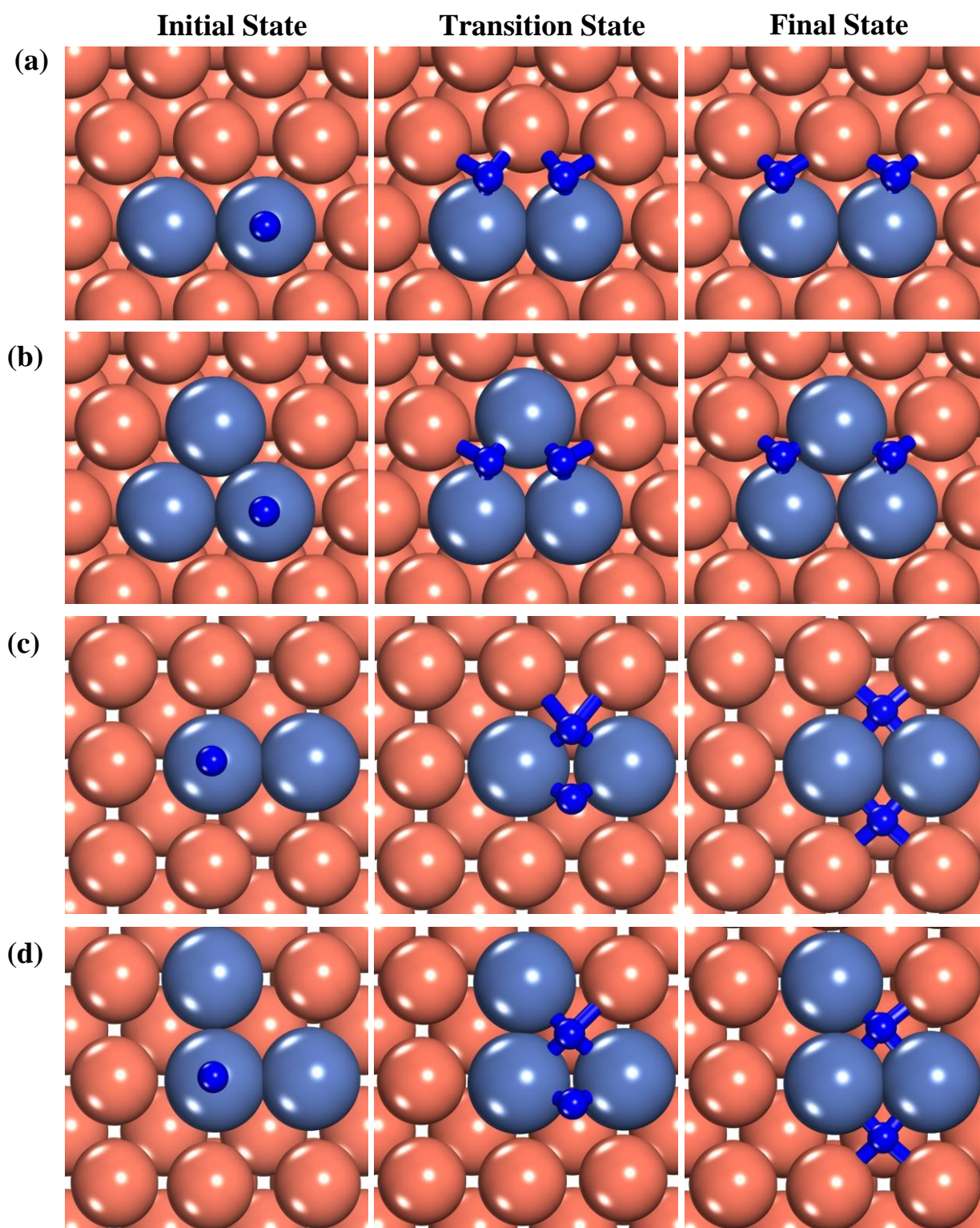


Figure S13. IS, TS and FS structures for the N_2 dissociation reaction on (a) $Ni_2Cu(111)$ surfaces; (b) $Ni_3Cu(111)$ surfaces; (c) $Ni_2Cu(100)$ surfaces and (d) $Ni_3Cu(100)$ surfaces. N atoms are shown in blue. The dopant and host metal atoms are shown in purple and orange, respectively.

VI. Initial final and transition state structures on pure metal surfaces- Association reactions

The following figures show the IS, TS and FS of the formation of NO, N₂ and CO₂ reaction on Rh, Cu and Ni pure metal surfaces.

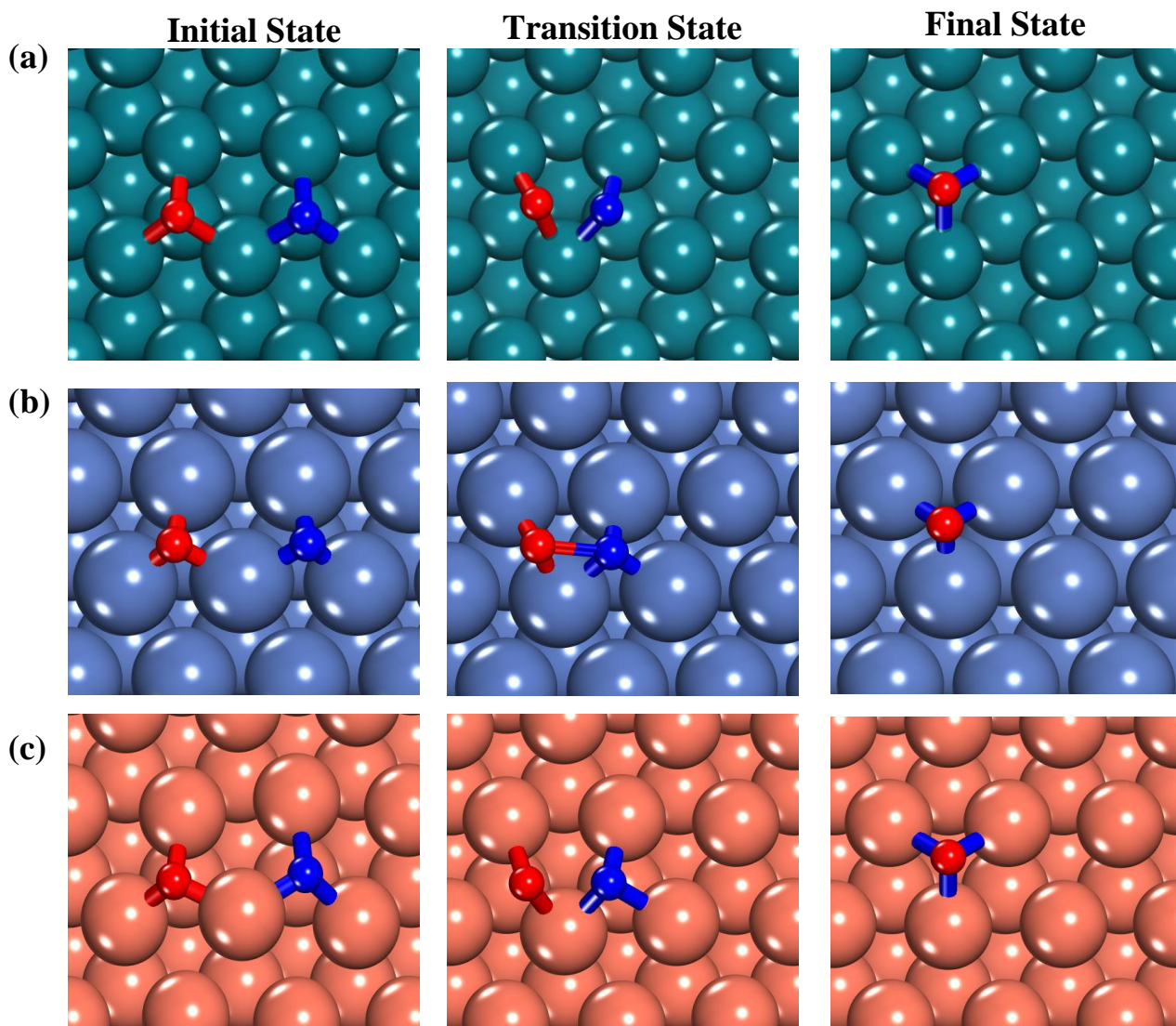


Figure S14. IS, FS and TS relaxed structures for the formation of NO on (a) Rh(111); (b) Ni(111) and (c) Cu(111). Ni, Cu and Rh atoms are shown in purple, orange and dark green, respectively. N and O atoms are shown in blue and red, respectively.

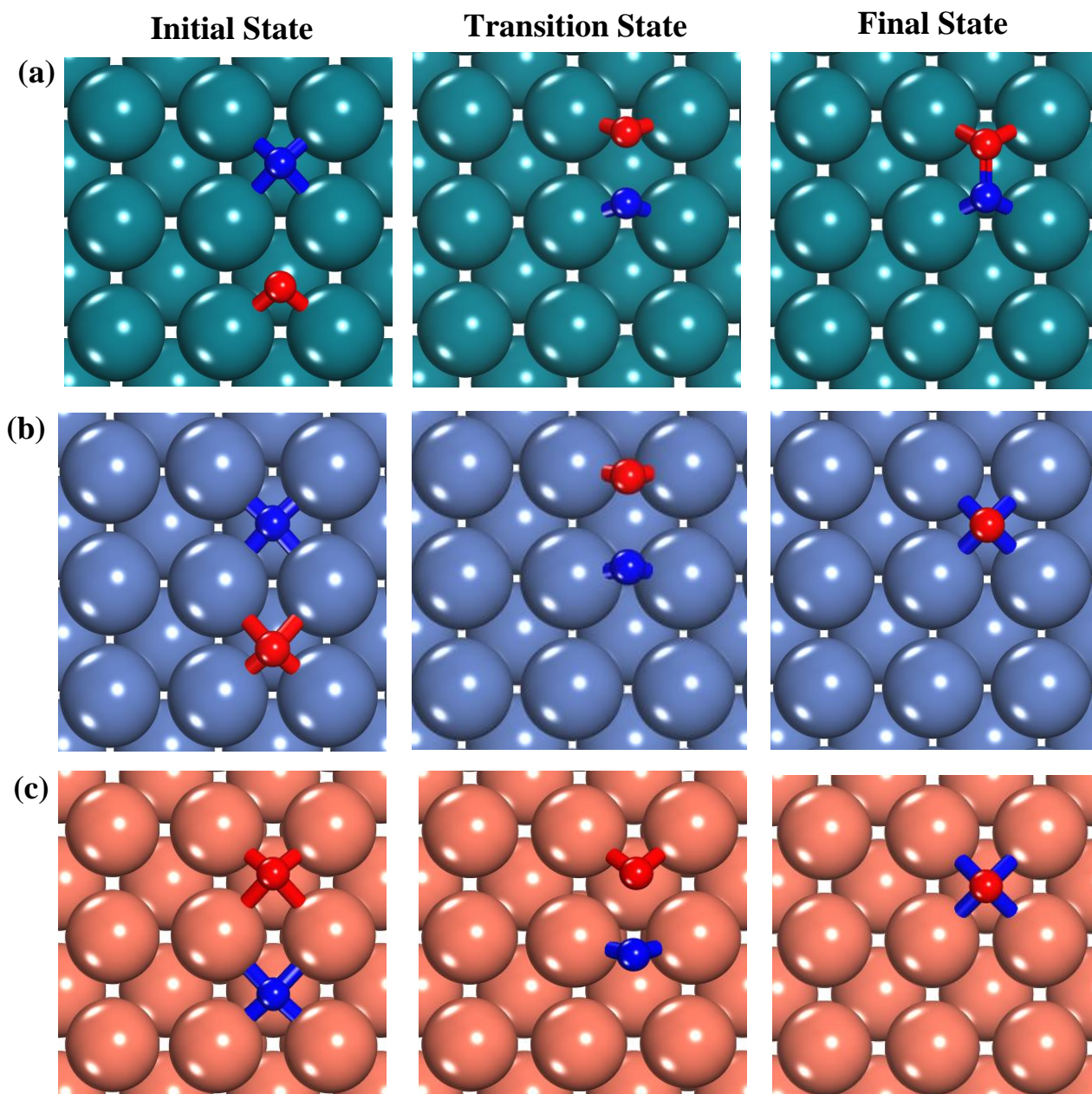


Figure S15. IS, FS and TS relaxed structures for the formation of NO on (a) Rh(100); (b) Ni(100) and (c) Cu(100). Ni, Cu and Rh atoms are shown in purple, orange and dark green, respectively. N and O atoms are shown in blue and red, respectively.

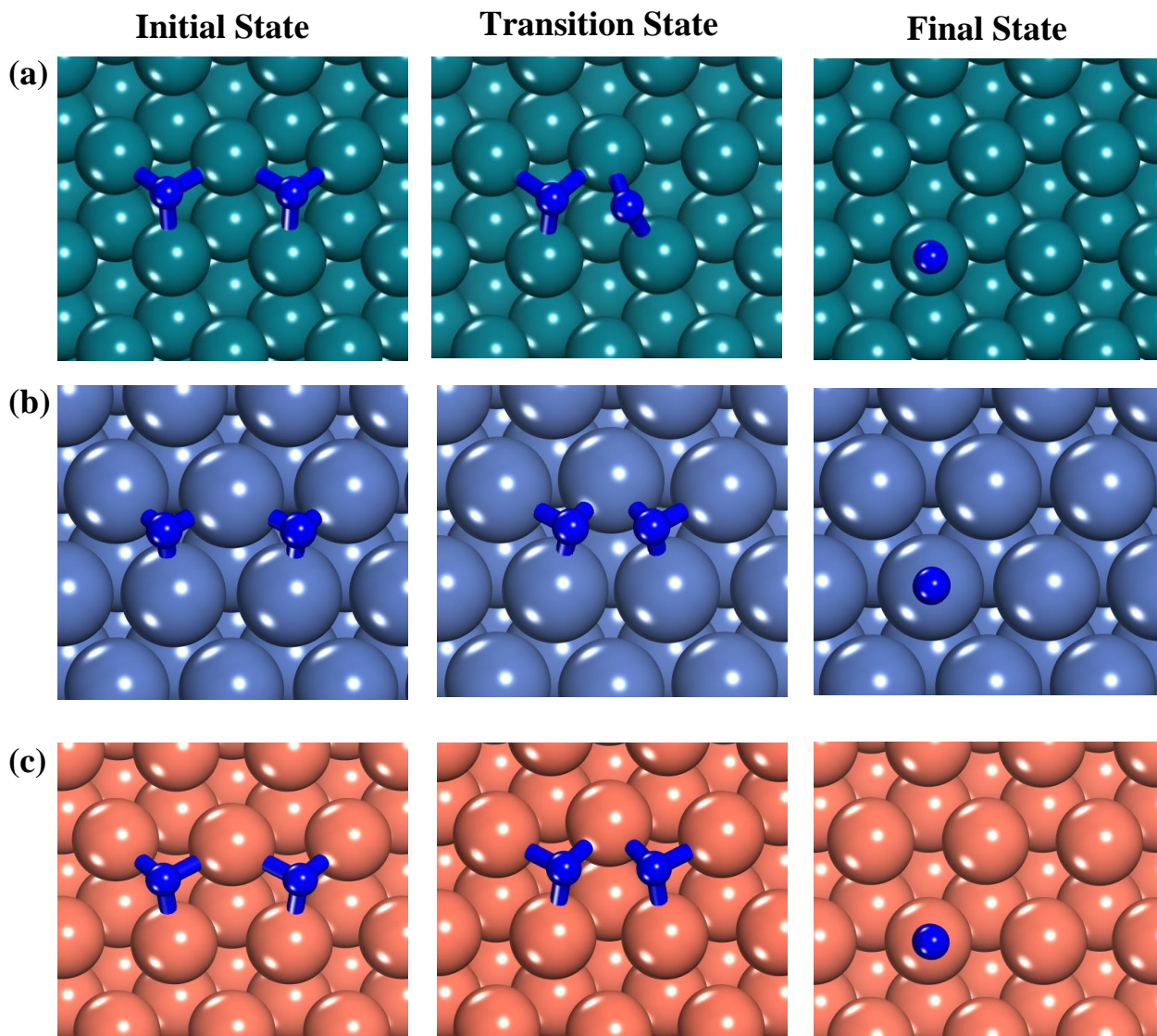


Figure S16. IS, FS and TS relaxed structures for the formation of N_2 on (a) Rh(111); (b) Ni(111) and (c) Cu(111). Ni, Cu and Rh atoms are shown in purple, orange and dark green, respectively. N atoms are shown in blue.

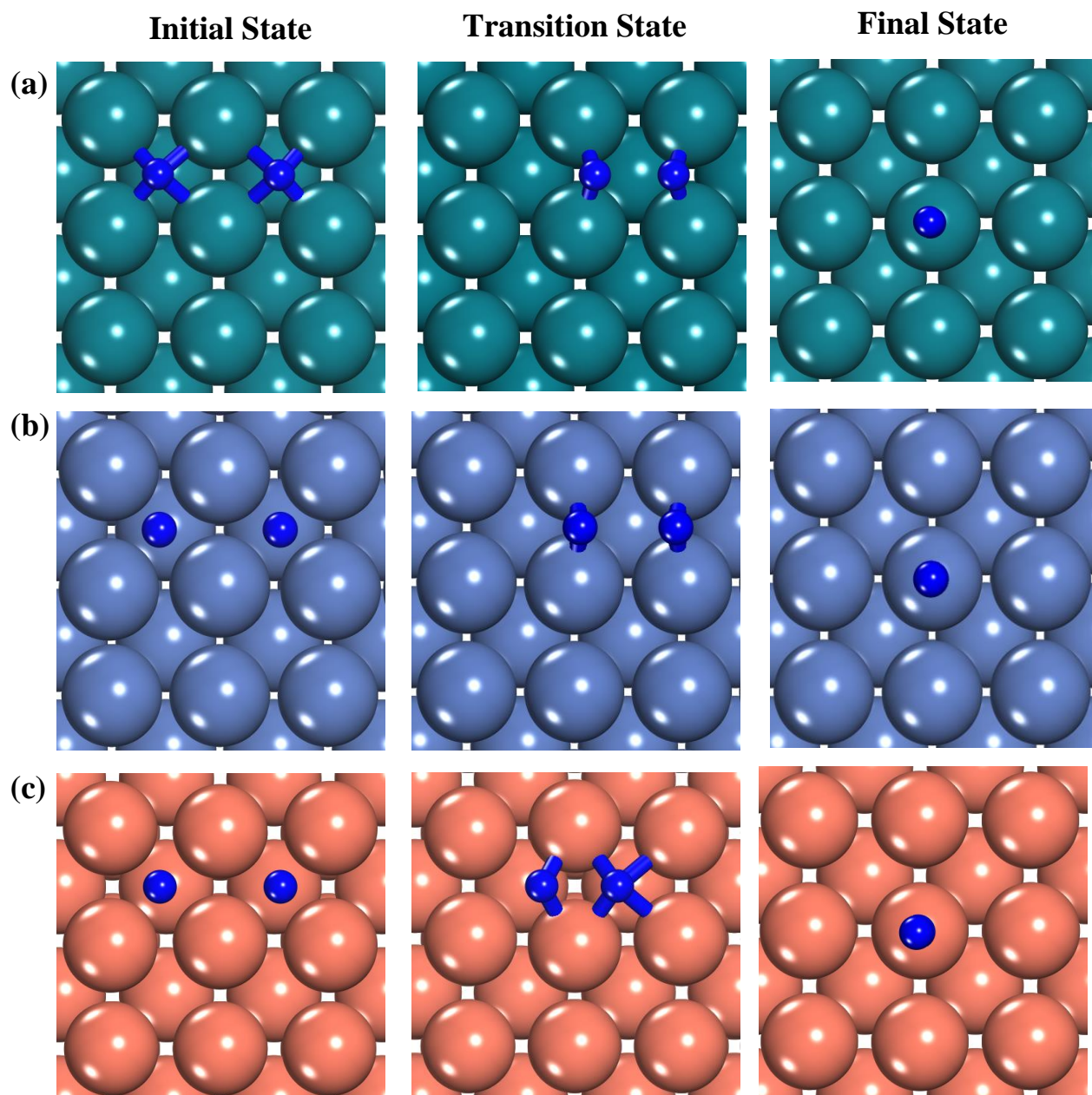


Figure S17. IS, FS and TS relaxed structures for the formation of N_2 on (a) Rh(100); (b) Ni(100) and (c) Cu(100). Ni, Cu and Rh atoms are shown in purple, orange and dark green, respectively. N atoms are shown in blue.

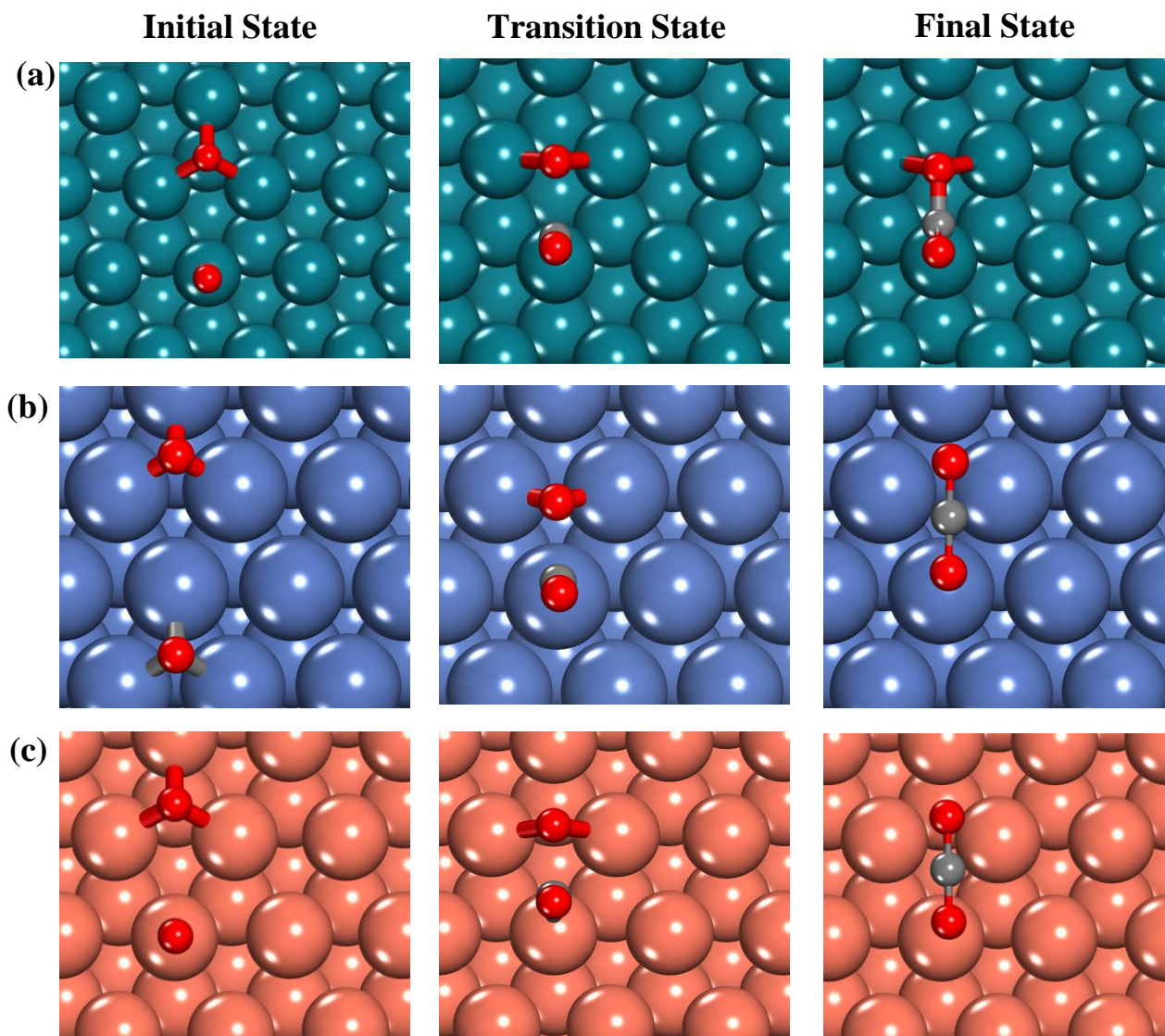


Figure S18. IS, FS and TS relaxed structures for the formation of CO₂ on (a) Rh(111); (b) Ni(111) and (c) Cu(111). Ni, Cu and Rh atoms are shown in purple, orange and dark green, respectively. O and C atoms are shown in red and grey, respectively.

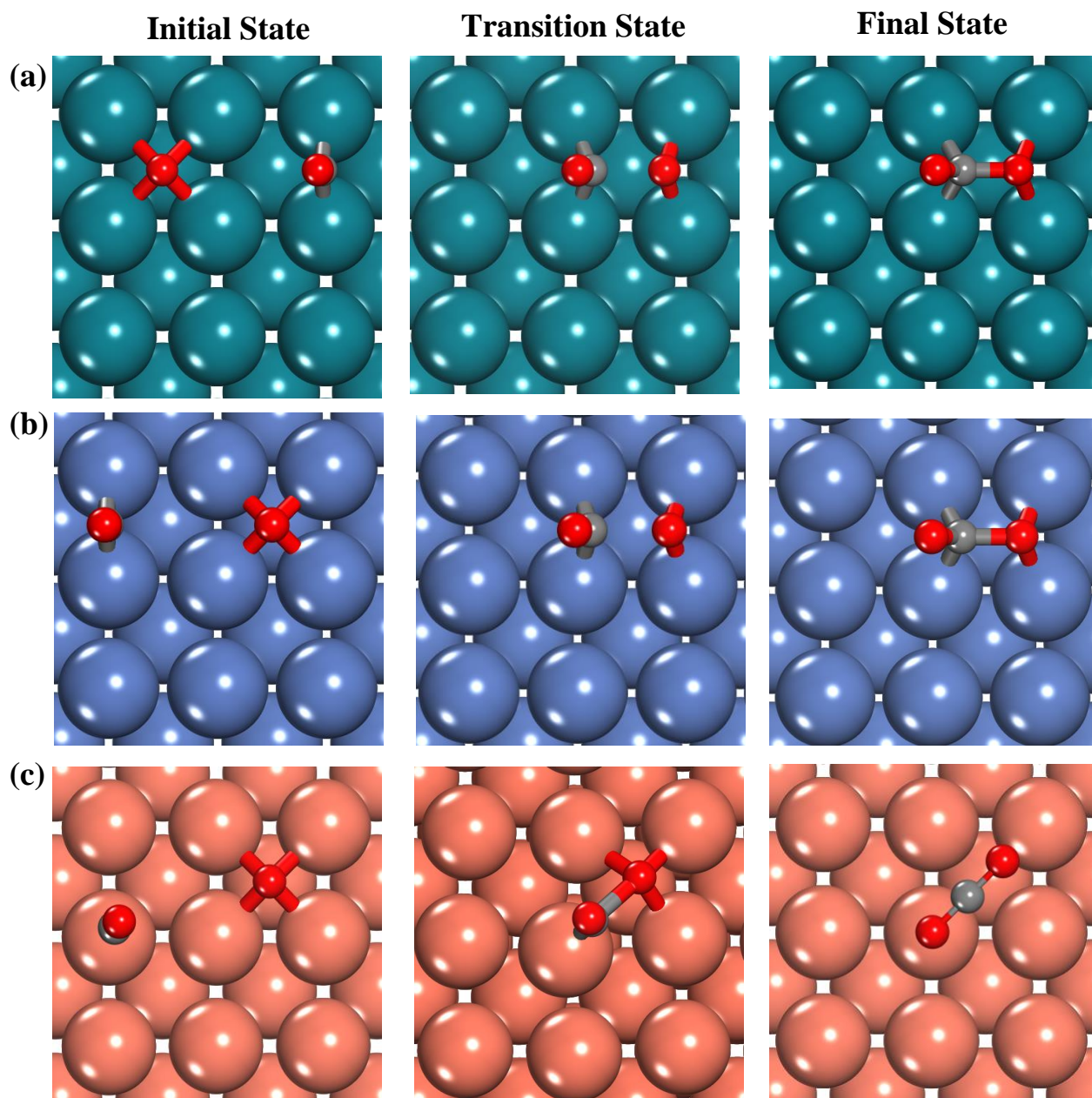


Figure S19. IS, FS and TS relaxed structures for the formation of CO₂ on (a) Rh(100); (b) Ni(100) and (c) Cu(100). Ni, Cu and Rh atoms are shown in purple, orange and dark green, respectively. O and C atoms are shown in red and grey, respectively.

VII. N₂ adsorption configuration on SAA surfaces

The most stable adsorption structure of N₂ on SAA and Ni/Cu dilute alloy surfaces is a linear upright configuration on a top site. This is also true for a number of pure metal surfaces such as Pd and Rh.^{3,4} Table S5 and

Table S6 display the computed adsorption energies for N₂ adsorbed in a perpendicular to the surface structure and a parallel to the surface structure on the studied (111) and (100) alloy surfaces, respectively.

Table S5. Adsorption energies of N₂ adsorbed in different configurations on (111) alloy surfaces. Dashes imply that the specific adsorption structure is not a minimum in the potential energy surface.

Alloy Surface	E _{ads} (N ₂) (eV)	
	Perpendicular Structure	Parallel Structure
NiAg(111)	-0.93	-0.19
NiAu(111)	-0.85	-0.08
NiCu(111)	-0.79	-0.08
PdAg(111)	-0.38	-0.17
PdAu(111)	-0.40	-0.18
PdCu(111)	-0.33	-0.16
PtAg(111)	-0.39	-0.17
PtAu(111)	-0.45	-0.18
PtCu(111)	-0.28	-0.16
RhAg(111)	-1.07	-0.36
RhAu(111)	-0.97	-0.25
RhCu(111)	-0.89	-0.24
Ni₂Cu(111)	-0.77	—
Ni₃Cu(111)	-0.75	-0.07

Table S6. Adsorption energies of N₂ adsorbed in different configurations on (100) alloy surfaces. Dashes imply that the specific adsorption structure is not a minimum in the potential energy surface.

Alloy Surface	E _{ads} (N ₂) (eV)	
	Perpendicular Structure	Parallel Structure
NiAg(100)	-0.97	-0.30
NiAu(100)	-0.93	-0.21
NiCu(100)	-0.89	-0.24
PdAg(100)	-0.43	—
PdAu(100)	-0.47	-0.18
PdCu(100)	-0.41	—
PtAg(100)	-0.43	—
PtAu(100)	-0.52	-0.18
PtCu(100)	-0.39	-0.16
RhAg(100)	-1.08	-0.42
RhAu(100)	-1.01	—
RhCu(100)	-0.94	—
Ni₂Cu(100)	-0.86	-0.22
Ni₃Cu(100)	-0.86	-0.21

VIII. Definition of the *effective* activation barrier

In Figure 2 and Figure 5 in the main text, we report *effective* activation barriers, for which the most stable structure is used as the IS. The concept of the effective activation barrier is better illustrated in Figure S20, where we show how the barrier predicted by the dimer method ($E_{a, \text{predicted}}$) and the reported effective barriers ($E_{a, \text{effective}}$) are calculated.

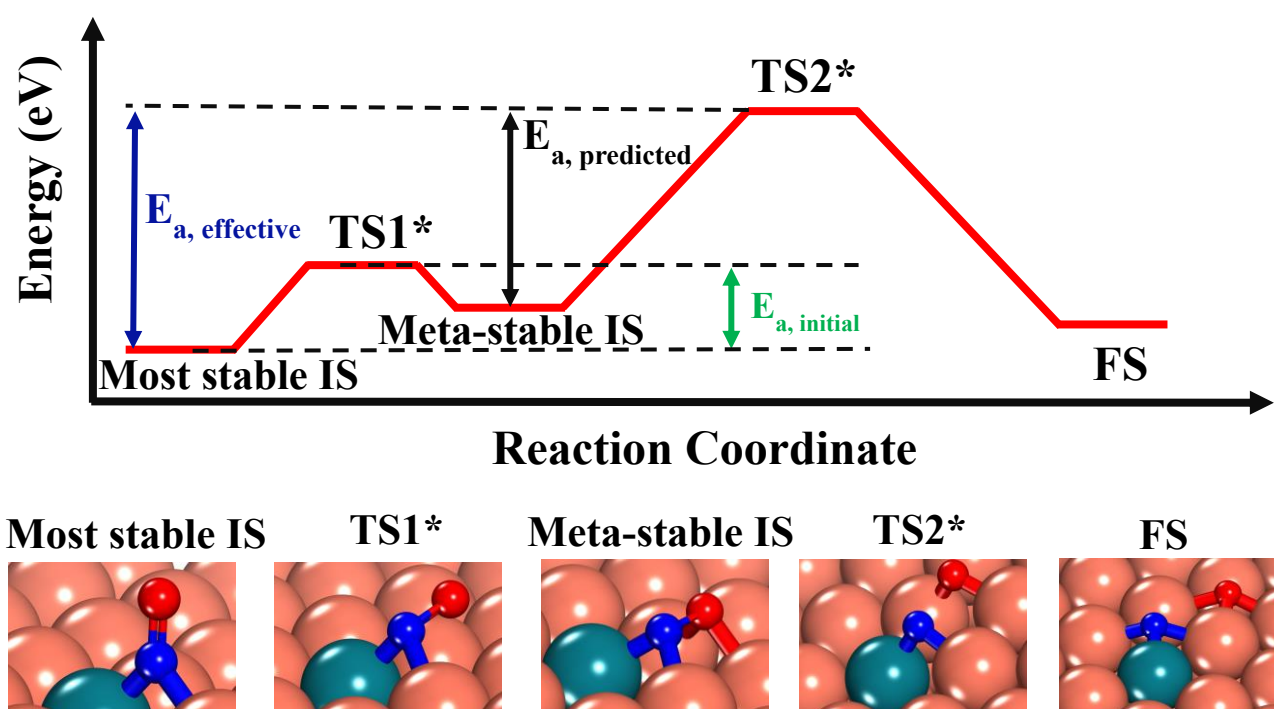


Figure S20. Illustration and definition of predicted and effective activation barriers. The effective activation barrier is always calculated with respect to the energetically most stable IS. The insets at the bottom of the figure show the corresponding structures of the presented potential energy surface for the dissociation of NO. O, N, Cu and dopant metal atoms are shown in red, blue, orange and green, respectively.

The dissociation of NO on Cu-based and platinum group metal (100) surfaces is an example of a system with a potential energy surface that resembles the one shown in Figure S20. More specifically, NO is initially adsorbed perpendicularly on a mixed bridge or a fourfold site (Most stable IS in Figure S20). Then, it tilts toward the surface, and ends up in an adsorption structure where the molecule is parallel to the surface (Meta-stable IS in Figure S20). Such “tilting processes” are activated and the corresponding kinetic barriers ($E_{a, \text{initial}}$ in Figure S20) are of similar magnitude to barriers noted for

diffusion processes (Table S7). Therefore, such events would be observed to be fast and quasi-equilibrated if one was to run e.g. a kinetic simulation. Finally, the N=O bond is cleaved (FS).

Table S7. Tilting barriers for a number of Cu-based and PGM surfaces.

Catalytic Surface	$E_{a, \text{initial}}$ (eV)
Ni/Cu(100)	0.28
Rh/Cu(100)	0.19
Pt/Cu(100)	0.19
Pd/Cu(100)	0.35
Pt(100)	0.40
Pd(100)	0.10
Rh(100)	0.24
Ni(100)	0.52
Cu(100)	0.45

IX. Summary of computed adsorption energies

The following tables summarise the adsorption energies of O, N₂ and NO on the top dopant site of SAA surfaces, and on the most stable sites of pure metal surfaces. The presented values are plotted in Figure 1 (a) in the main text.

Table S8. Adsorption energies of NO on the top dopant site on SAA surfaces and on the most stable (i.e. threefold fcc) site of pure metal surfaces.

Catalytic Surface	E_{ads}(NO) (111) (eV)	E_{ads}(NO) (100) (eV)
NiAg	-2.30	-2.35
NiAu	-2.13	-2.32
NiCu	-2.09	-2.25
PdAg	-1.18	-1.24
PdAu	-1.13	-1.30
PdCu	-1.06	-1.21
PtAg	-1.38	-1.47
PtAu	-1.36	-1.58
PtCu	-1.22	-1.42
NiAg	-2.58	-2.68
NiAu	-2.44	-2.66
NiCu	-2.31	-2.48
Au	-0.85	-0.58
Ag	-0.82	-0.68
Cu	-1.55	-1.61
Pt	-2.25	-2.70
Rh	-2.84	-2.87
Ni	-2.84	-2.99
Pd	-2.62	-2.40

Table S9. Adsorption energies of N₂ on the top dopant site on SAA surfaces and on the most stable (i.e. atop) site of pure metal surfaces.

Catalytic Surface	E_{ads}(N₂) (111) (eV)	E_{ads}(N₂) (100) (eV)
NiAg	-0.93	-0.97
NiAu	-0.85	-0.93
NiCu	-0.79	-0.89
PdAg	-0.38	-0.42
PdAu	-0.40	-0.46
PdCu	-0.32	-0.41
PtAg	-0.39	-0.43
PtAu	-0.45	-0.52
PtCu	-0.28	-0.39
NiAg	-1.07	-1.08
NiAu	-0.97	-1.00
NiCu	-0.90	-0.93
Au	-0.17*	-0.16*
Ag	-0.15*	-0.16*
Cu	-0.15	-0.30
Pt	-0.45	-0.70
Rh	-0.79	-0.80
Ni	-0.65	-0.79
Pd	-0.48	-0.61

* physisorption: N₂ is far above the top layer of the surface.

Table S10. Adsorption energies of O on the top dopant site on SAA surfaces and on the most stable (i.e. atop) site of pure metal surfaces.

Catalytic Surface	$E_{\text{ads}}(\text{O})$ (111) (eV)	$E_{\text{ads}}(\text{O})$ (100) (eV)
NiAg	-1.12	-1.25
NiAu	-0.47	-0.65
NiCu	-0.83	-0.99
PdAg	0.13	0.04
PdAu	0.56	0.45
PdCu	0.32	0.21
PtAg	-0.28	-0.33
PtAu	0.03	-0.17
PtCu	-0.08	-0.30
NiAg	-0.98	-1.27
NiAu	-0.64	-0.96
NiCu	-0.74	-1.02
Au	-0.20	-0.20
Ag	-0.60	-1.05
Cu	-1.90	-3.20
Pt	-1.52	-1.06
Rh	-2.28	-2.30
Ni	-2.47	-2.94
Pd	-1.49	-1.46

References

- 1 H. Thirumalai and J. R. Kitchin, *Top. Catal.*, 2018, **61**, 462–474.
- 2 M. T. Darby, R. Réocreux, E. C. H. Sykes, A. Michaelides and M. Stamatakis, *ACS Catal.*, 2018, **8**, 5038–5050.
- 3 M. Mavrikakis, J. Rempel, J. Greeley, L. B. Hansen and J. K. Nørskov, *J. Chem. Phys.*, 2002, **117**, 6737–6744.
- 4 B. Hammer, *J. Catal.*, 2001, **199**, 171–176.